

Identification of orbital pumping from spin pumping and rectification effects

Nils Keller,^{1,2,*} Arnab Bose,^{1,3,*} Nozomi Soya,^{2,*} Elias Hauth,^{1,2} Fabian Kammerbauer,¹ Rahul Gupta,¹ Hiroki Hayashi,² Hisanobu Kashiki,² Gerhard Jakob,¹ Sachin Krishna,^{1,†} Kazuya Ando,^{2,4,5,‡} and Mathias Kläui^{1,6,7,8}

¹*Institute of Physics, Johannes Gutenberg University Mainz, Staudingerweg 7, 55128 Mainz, Germany*

²*Department of Applied Physics and Physico-Informatics, Keio University, Yokohama 223-8522, Japan*

³*Department of Electrical Engineering, Indian Institute of Technology Kanpur, 208016, India*

⁴*Keio Institute of Pure and Applied Science (KiPAS), Keio University, Yokohama 223-8522, Japan*

⁵*Center for Spintronics Research Network (CSRN), Keio University, Yokohama 223-8522, Japan*

⁶*Graduate School of Excellence Materials Science in Mainz, 55099, Mainz, Germany*

⁷*Department of Physics, Center for Quantum Spintronics,*

Norwegian University of Science and Technology, 7491, Trondheim, Norway

(Dated: February 13, 2025)

The recently predicted mechanism of orbital pumping enables the generation of pure orbital current from a precessing ferromagnet (FM) without the need for electrical current injection. This orbital current can be efficiently injected into an adjacent nonmagnetic material (NM) without being hampered by electrical conductivity mismatch. However, experimentally identifying this novel effect presents significant challenges due to the substantial background contributions from spin pumping and spin rectification effects (SREs). In this work, we disentangle the effects of orbital pumping from spin pumping in bilayer structures composed of Nb/Ni and Nb/Fe₆₀Co₂₀B₂₀ by observing a sign reversal of the measured voltage. This reversal arises from the competing signs of the spin and orbital Hall effects in the Nb. We establish methods to differentiate the pumping signal from SREs by analyzing the distinct angular dependence of the measured voltage and its spatial dependence relative to the radio frequency excitation source.

INTRODUCTION

Spin and orbital angular momentum are two fundamental properties of electrons, interconnected through spin-orbit coupling (SOC). In spintronics, the SOC is essential in the emergence of various intriguing physical phenomena [1] such as stabilization of chiral magnetic skyrmions [2–5] and spin current generation mechanisms [6]. The study of spin currents (J_S), including those generated via the spin Hall effect (SHE) [7–10] and the Rashba-Edelstein effect (REE) [11, 12], has been a central focus in spintronics, especially due to its potential applications in nonvolatile magnetic random-access memory (MRAM) [13, 14].

Recent interest has shifted toward the generation of orbital currents (J_O) due to its potential applications in energy efficient MRAM technology [15, 16]. Theoretical studies suggest that orbital current is a fundamental entity that can for instance result in spin current leveraging the SOC of materials [16–18]. A major advantage of orbital currents is their potential to be orders of magnitude larger than spin currents across a wide range of materials [19], as they are not inherently limited by the relativistic SOC. Consequently, orbital currents could overcome the limitations of spin currents, particularly in terms of scalability and efficiency, making them highly promising for memory and logic applications [16].

Thus far, the emerging field of orbitronics has mainly focused on the generation of J_O through the orbital Hall effect (OHE) [20–27] and the orbital Rashba-Edelstein effect (OREE) [28–32]. Recently, theorists have predicted the effect of "orbital pumping", where a precess-

ing magnet can emit a significant orbital current without requiring an associated electric current (Figure 1 (a)) [33–35]. This effect is analogous to the previously demonstrated spin pumping effect, where a precessing magnet emits pure spin current [36–41] (Figure 1 (b)).

Both spin and orbital pumping provide methods to generate spin and orbital currents without the challenges posed by electrical conductivity mismatch and enable easy and clear detection in comparatively simple samples [42]. As illustrated in Figure 1 (a,b), the emitted orbital and spin currents are converted into a transverse voltage in the adjacent nonmagnet via reciprocal effects known as the inverse orbital Hall effect (IOHE), the inverse orbital Rashba-Edelstein effect [31, 43–45] and the inverse spin Hall effect (ISHE) and inverse Rashba-Edelstein effect [46, 47], respectively. However, in real systems, these processes can occur simultaneously, along with spin-rectification effects (SREs) arising from the interplay between time-varying magnetoresistance and the applied oscillating field. This overlap makes it highly challenging to isolate the orbital pumping signal from the often dominant background contributions of spin pumping and SREs and so methods are needed to identify orbital pumping unambiguously.

In this work, we demonstrate that we can obtain a clear distinction of orbital pumping by carefully selecting materials with opposing signs of the OHE and SHE and by performing rigorous angular-dependent measurements of the pumped voltage signal. This is achieved using devices specifically designed to produce a more uniform radio frequency (RF) field while minimizing other parasitic effects as discussed in subsequent sec-

tions (Figure 1 (c)).

EXPERIMENT

We have prepared four primary series of samples using a Singulus Rotaris tool via magnetron sputtering on undoped Si/SiO₂ substrates: (1) Sub/Ta(1)/Nb(4)/Ni(3, 6, 10, 15)/cap, (2) Sub/Ta(1)/Pt(4)/Ni(3, 6, 10, 15)/cap, (3) Sub/Ta(1)/Nb(4)/Fe₆₀Co₂₀B₂₀(8)/cap, and (4) Sub/Ta(1)/Pt(4)/Fe₆₀Co₂₀B₂₀(8)/cap. Here, the numbers in parentheses are the nominal thicknesses in nm, and the cap is MgO(1.5)/Ta(1.5) to protect the samples from oxidation. We fabricate the devices shown in Figure 1 (c) through successive cycles of electron beam lithography, Ar⁺ milling, RF magnetron sputtering, and lift-off techniques. More information on sample preparation and fabrication is provided in the supplementary information (SI1).

A schematic diagram of the device is shown in Figure 1 (c). It consists of a coplanar waveguide, with a narrow and long non-magnetic (NM)/ferromagnetic (FM) wire placed in the slots of the waveguide with a length of 200 μm and a width of 8 μm. The waveguide and the NM/FM device, together with the contacts, are electrically isolated by inserting an SiO₂ layer. The central concept is to pass an RF current through the waveguide, producing an RF magnetic field that drives the magnet into resonance. As a result, the magnet emits both orbital and spin currents into the adjacent NM layer, such as Nb, Pt, or Ru, which are then converted into a direct current (DC) voltage due to the IOHE and ISHE (Figure 1 (a,b)).

We chose Nb and Pt as they exhibit opposite signs for the spin Hall angle (SHA), yet have the same sign for the orbital Hall angle (OHA) [24] from which we can separate the orbital and spin pumping effects via sign reversal. The ferromagnetic materials Ni and FeCoB are selected due to their contrasting abilities to detect orbital currents [22, 24]. Due to the Onsager reciprocity Ni is therefore expected to generate a pronounced orbital current from the orbital pumping as compared to FeCoB [33, 34]. The Nb- and Pt-based samples are the central focus of this work as they facilitate the unambiguous detection of orbital pumping in our setup via sign reversal in the measured voltage. For comparison, the pumping signal into Ru, another candidate known for exhibiting strong OHE and weak SHE [15, 24] is also analyzed in the Sub/Ta(1)/Ru(4)/Ni(10)/cap stack (see supplementary information).

The experiment is performed by sweeping an external magnetic field (H) at an angle ϕ relative to the x -axis, and measuring the voltage in the NM/FM wire, as shown in Figure 1 (c). This voltage is fitted using symmetric (V_S) and anti-symmetric (V_A) Lorentzian functions [39, 40, 46]. In the absence of other SREs, V_S corresponds to the spin/orbital pumping signal, which

can be unambiguously identified via sign reversal in our measurements due to the competing sign of SHA and OHA in Nb [24].

While the spin (and orbital) pumping effects are expected to generate only V_S , previous experiments have provided significant evidence for a non-zero value of V_A [39, 40, 46]. This observation is often attributed to SREs, primarily arising from the induced RF current within the device (Figure 1 (c)), which couples with the oscillating magnetoresistance as the FM oscillates at ferromagnetic resonance. Consequently, it is critical to determine whether SREs also generate V_S , as this would complicate the analysis of spin and orbital pumping, potentially leading to incorrect or ambiguous interpretations. One possible origin of V_S is the conventional spin-torque ferromagnetic resonance (ST-FMR) [48], caused by the induced RF current flowing through the device. This mechanism, which can produce a significant V_S , has largely been overlooked in previous studies [38-40, 45, 46].

To address this issue, we have fabricated the NM/FM device within the slot of a waveguide (Figure 1 (c)). This configuration allows us to distinguish the pumping signal from other SREs, which is not feasible when the device is positioned on top of the waveguide, as commonly practiced in earlier studies [49]. In our geometry, the V_S exhibits the following angular dependence as a function of the in-plane magnetic field (H) applied at an angle, ϕ from the device long axis.

$$V_S(\phi) \approx V_S^{\text{pump}} \sin \phi + V_{S, \text{AMR}}^{\text{ST-FMR}} \cos \phi \sin 2\phi + V_{S, \text{AMR}}^{\text{NL}} \sin 2\phi \quad (1)$$

In this work, we primarily focus on the coefficient of V_S^{pump} in different samples, which represents the strength of the pumping signal. $V_{S, \text{AMR}}^{\text{ST-FMR}}$ accounts for contributions from conventional ST-FMR, arising from the induced RF current and the anisotropic magnetoresistance (AMR) effect as discussed before. $V_{S, \text{AMR}}^{\text{NL}}$ originates from nonlocal ST-FMR, where the induced RF current couples with out-of-plane magnetization oscillations driven by the Oersted field of the waveguide. Additional minor components of V_S , which are negligible in our work, and the origins of V_A are discussed in detail in the supplementary information.

RESULTS AND DISCUSSION

Figure 2 presents the central results of this work. Figures 2 (a-d) show the typical voltage spectrum (black squares) in our pumping experiment, fitted with a superposition of symmetric (V_S) (blue) and anti-symmetric Lorentzian functions (V_A) (red). The fit is displayed in green. The fitting procedure also includes a constant and linear term. The general fitting procedure

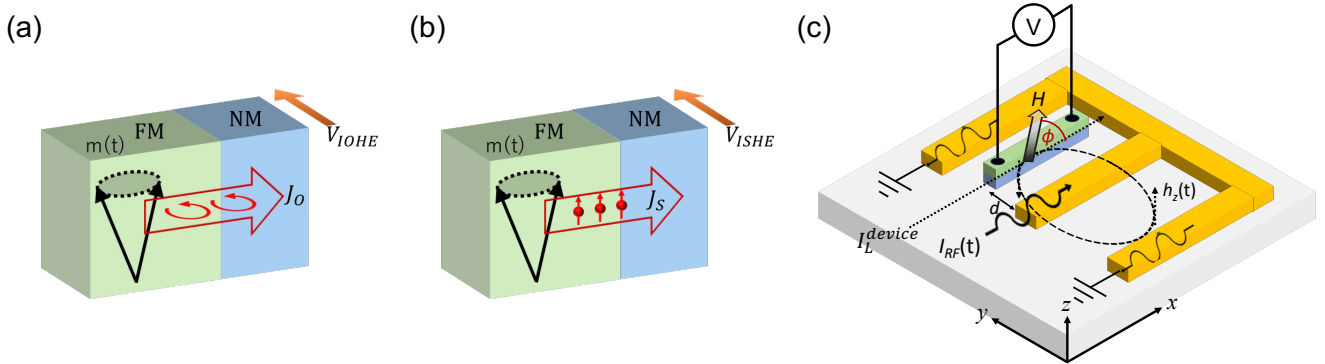


Figure 1. Schematic representation of (a) orbital pumping and (b) spin pumping from a precessing magnet into an adjacent NM metal. The orbital and spin currents generated by the precession of the magnet induce a transverse voltage via the IOHE and ISHE. (c) Schematic illustration of the device and experimental set up. The RF current (I_{RF}) flowing through the waveguide generates an RF Oersted field h_z on the NM/FM device. A fraction of the applied RF current is induced in the device (I_L^{device}) flowing along the longitudinal x -direction. Additionally, a static magnetic field H is applied in the plane of the device with an angle ϕ with respect to the x -axis. The angle convention is chosen such that rotating in the mathematical positive direction increases the value of the angle. The voltage resulting from the orbital and/or spin pumping is measured along the sample wire.

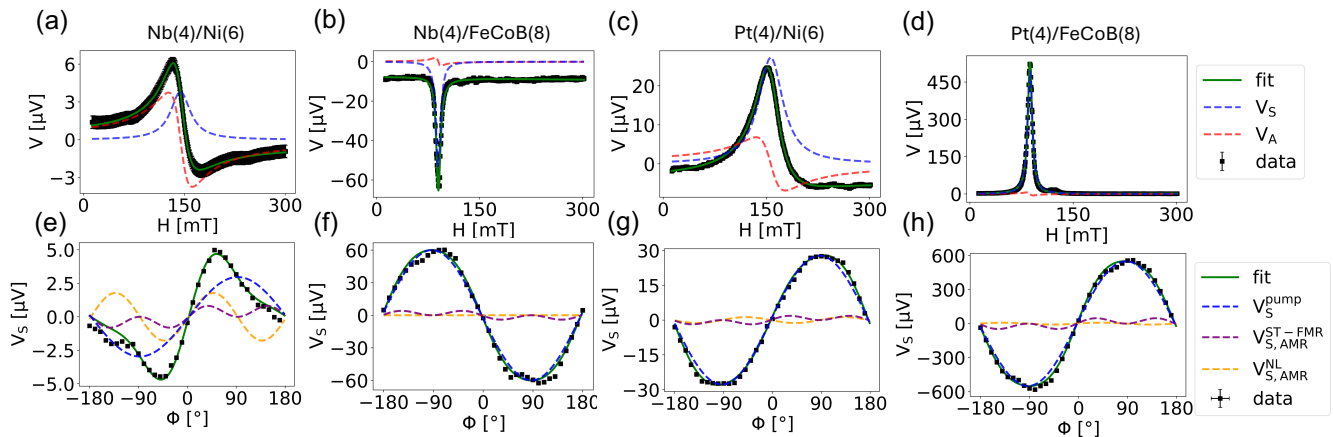


Figure 2. Magnetic field sweep measurements for (a) Nb(4)/Ni(6), (b) Nb(4)/FeCoB(8), (c) Pt(4)/Ni(6) and (d) Pt(4)/FeCoB(8) for a gap width of $6 \mu\text{m}$ and an angle of 80° . The data are fitted with a superposition of symmetric (blue) and antisymmetric (red) Lorentzians. (e-h) The extracted values for V_S are plotted as a function of the angle of the swept magnetic field. The data are fitted according to Equation (1).

ture is discussed in the supplementary information (SI2) in detail. The sign of V_S in Pt/Ni (Figure 2 (c)) and Pt/FeCoB (Figure 2 (d)) reflects the widely studied spin pumping effect in Pt [38–40, 46]. Most interestingly, we observe a sign reversal in V_S for Nb/Ni (Figure 2 (a)) compared to Nb/FeCoB (Figure 2 (b)), which cannot be explained by the conventional spin pumping effect. We find that the sign of V_S in Nb/FeCoB (Figure 2 (b)) is opposite to that in Pt (Figure 2 (c, d)), suggesting that the sign of ISHE in Nb is opposite to that in Pt, consistent with theoretical predictions [19] and our previous work [24]. In contrast, the observed same sign of V_S in Nb/Ni (Figure 2 (a)) and Pt/(Ni or FeCoB) (Figures 2 (c,d)) strongly suggests that the orbital pumping effect dominates in the Nb/Ni samples where the injected or-

bitral current is converted into an electrical voltage via the IOHE.

Next, we analyze the influence of other SREs on our measurements by studying the angular dependence of V_S , as shown in Figures 2 (e-h). We observe that V_S can be reasonably well fitted with Equation (1), indicating a prominent contribution from spin and orbital pumping ($\sin \phi$ term) along with non-zero values of other SREs across all samples. These findings confirm that the sign of the SHA is negative for Nb and it is positive for Pt (compare Figures 2 (f, g, h)). Further, the angular dependence reveals that the pumping signal ($\sin \phi$ term in V_S) in Nb/Ni is positive (2 (e)), indeed predominantly driven by orbital pumping prevailing over spin pumping.

Our work demonstrates that SREs are stronger in

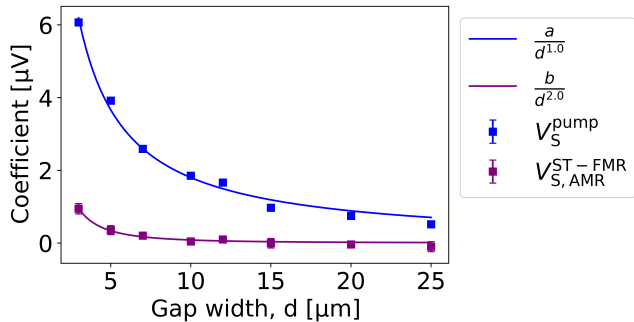


Figure 3. The strengths of the different effects in Nb(4)/Ni(10) bilayers are characterized by the coefficients from Equation (1). The coefficients are plotted as a function of the gap width, d . The V_S^{pump} data is fitted with $\frac{a}{d^m}$ obtaining a value of $m \approx 1.0$ for the best fit.

Ni-based samples than in FeCoB films, as Ni exhibits the highest AMR among other transition metal magnets (Co, Fe). This enhanced AMR leads to more significant SREs from the undesired spin and orbital currents, and various current-induced magnetic fields (more details are provided in the supplementary information SI3). The sign reversal of the $\sin \phi$ term, clearly, allows us to detect orbital pumping via the IOHE. We also conducted an analogous experiment in Ru/Ni (see supplementary information SI4) that shows large signals from orbital pumping due to the vanishingly small SHA and the predicted large OHA [24].

Building upon these observations, we investigate the dependence of the pumping effect and SREs on the gap width (d) between the device and the waveguide in Nb(4)/Ni(10) samples (Figure 3). The individual data points are obtained using Equation (1). We find that the pumping signal (V_S^{pump} , blue curve in Figure 3) goes down as d increases and is proportional to $\frac{1}{d^m}$ with $m \approx 1.0$ in our work. Since the spin-pumping voltage is proportional to the power of the microwave magnetic field, it should scale with $\frac{1}{d^2}$. However, due to the finite size of the waveguide and the device a behaviour of $m < 2$ is expected. The voltage component arising from $V_{S,AMR}^{\text{ST-FMR}}$ also follows a similar trend (purple squares in Figure 3) but exhibits a steeper decrease with $m \approx 2.0$. Such a steep decrease in $V_{S,AMR}^{\text{ST-FMR}}$ is expected as it results from the interplay between the induced RF current and its Oersted field within the device, both of which diminish as the spacing increases. We find a similar behaviour in the bilayer system Ru(4)/Ni(10) (see supplementary information SI5). Thus, our findings demonstrate that the spacing dependence is an efficient way to separate the pumping signal from other SREs.

SUMMARY AND CONCLUSION

In this work, we systematically investigate spin and orbital pumping effects in Nb/Ni and Nb/FeCoB bilayers, comparing our findings with those from Pt/Ni and Pt/FeCoB systems. We examine the DC voltage spectrum generated by orbital and spin pumping, along with other rectification effects, under uniform microwave excitation, ensured by positioning the lithographically fabricated bilayer device within the waveguide slot. Our methodology includes analyzing the angular dependence of the measured voltage signal as a function of the in-plane magnetic field (Figure 2), as well as its variation with the separation between the waveguide and the device (Figure 3). This approach enables us to uniquely distinguish the pumping signal from undesired additional rectification effect signal contributions. We confirm the orbital pumping effect by observing the sign reversal of the $\sin \phi$ component of the symmetric Lorentzian voltage signal in Nb/Ni compared to Nb/FeCoB and its spacing dependence, which provides a distinct signature from spin rectification effects. Thus, we not only demonstrate an efficient method to generate orbital current via the "orbital pumping" mechanism from a precessing magnet but also establish a robust approach to disentangle it from spin pumping and other rectification effects.

ACKNOWLEDGEMENT

The authors thank the DFG (Spin+X (A01, A11, B02) TRR 173-268565370 and Project No. 358671374), the Horizon 2020 Framework Programme of the European Commission under FETOpen Grant Agreement No. 863155 (s-Nebula); the European Research Council Grant Agreement No. 856538 (3D MAGiC); and the Research Council of Norway through its Centers of Excellence funding scheme, Project No. 262633 "QuSpin". The study also has been supported by the European Horizon Europe Framework Programme under an EC Grant Agreement N°101129641 "OBELIX". AB acknowledges the support from the Alexander von Humboldt Foundation for his postdoctoral fellowship. KA acknowledges the support from JSPS KAKENHI (Grant No. 22H04964), Spintronics Research Network of Japan (Spin-RNJ), and MEXT Initiative to Establish Next-generation Novel Integrated Circuits Centers (X-NICS) (Grant No. JPJ011438).

Author contributions

The samples were grown by FK, RG and GJ and the devices were fabricated by NK and NS with inputs of AB. NK and EH carried out the experiments and an-

alyzed the data with inputs from AB who conceived the idea. SK and GJ assisted in the experiments and also in data analysis. HK and HH assisted in theory. The manuscript was written by AB, NK, and SK. The whole project was supervised by KA and MK. All authors commented on the manuscript.

Data Availability

Data is made available from the corresponding author upon reasonable request.

* These authors contributed equally to this work.

† krishnia@uni-mainz.de

‡ ando@appi.keio.ac.jp

§ klaui@uni-mainz.de

- [1] A. Soumyanarayanan, N. Reyren, A. Fert, and C. Panagopoulos, “Emergent phenomena induced by spin-orbit coupling at surfaces and interfaces,” *Nature*, vol. 539, pp. 509–517, Nov 2016.
- [2] S. Woo, K. Litzius, B. Krüger, M.-Y. Im, L. Caretta, K. Richter, M. Mann, A. Krone, R. M. Reeve, M. Weigand, P. Agrawal, I. Lemesh, M.-A. Mawass, P. Fischer, M. Kläui, and G. S. D. Beach, “Observation of room-temperature magnetic skyrmions and their current-driven dynamics in ultrathin metallic ferromagnets,” *Nat. Mater.*, vol. 15, pp. 501–506, May 2016.
- [3] A. Fert, V. Cros, and J. Sampaio, “Skyrmions on the track,” *Nat. Nanotechnol.*, vol. 8, pp. 152–156, Mar 2013.
- [4] A. Thiaville, S. Rohart, Émilie Jué, V. Cros, and A. Fert, “Dynamics of dzyaloshinskii domain walls in ultrathin magnetic films,” *Europhys. Lett.*, vol. 100, p. 57002, dec 2012.
- [5] K. Everschor-Sitte, J. Masell, R. M. Reeve, and M. Kläui, “Perspective: Magnetic skyrmions—Overview of recent progress in an active research field,” *J. Appl. Phys.*, vol. 124, p. 240901, 12 2018.
- [6] A. Manchon, J. Železný, I. M. Miron, T. Jungwirth, J. Sinova, A. Thiaville, K. Garello, and P. Gambardella, “Current-induced spin-orbit torques in ferromagnetic and antiferromagnetic systems,” *Rev. Mod. Phys.*, vol. 91, p. 035004, Sep 2019.
- [7] J. E. Hirsch, “Spin hall effect,” *Phys. Rev. Lett.*, vol. 83, pp. 1834–1837, Aug 1999.
- [8] J. Sinova, S. O. Valenzuela, J. Wunderlich, C. H. Back, and T. Jungwirth, “Spin hall effects,” *Rev. Mod. Phys.*, vol. 87, pp. 1213–1260, Oct 2015.
- [9] I. M. Miron, K. Garello, G. Gaudin, P.-J. Zermatten, M. V. Costache, S. Auffret, S. Bandiera, B. Rodmacq, A. Schuhl, and P. Gambardella, “Perpendicular switching of a single ferromagnetic layer induced by in-plane current injection,” *Nature*, vol. 476, pp. 189–193, Aug 2011.
- [10] L. Liu, C.-F. Pai, Y. Li, H. W. Tseng, D. C. Ralph, and R. A. Buhrman, “Spin-torque switching with the giant spin hall effect of tantalum,” *Science*, vol. 336, no. 6081, pp. 555–558, 2012.
- [11] Y. A. Bychkov and É. I. Rashba, “Properties of a 2D electron gas with lifted spectral degeneracy,” *Soviet Journal of Experimental and Theoretical Physics Letters*, vol. 39, p. 78, Jan. 1984.
- [12] A. Manchon, H. C. Koo, J. Nitta, S. M. Frolov, and R. A. Duine, “New perspectives for rashba spin-orbit coupling,” *Nat. Mater.*, vol. 14, pp. 871–882, Sep 2015.
- [13] S. Bhatti, R. Sbiaa, A. Hirohata, H. Ohno, S. Fukami, and S. Piramanayagam, “Spintronics based random access memory: a review,” *Mater. Today*, vol. 20, no. 9, pp. 530–548, 2017.
- [14] B. Dieny, I. L. Prejbeanu, K. Garello, P. Gambardella, P. Freitas, R. Lehnendorff, W. Raberg, U. Ebels, S. O. Demokritov, J. Akerman, A. Deac, P. Pirro, C. Adelman, A. Anane, A. V. Chumak, A. Hirohata, S. Mangin, S. O. Valenzuela, M. C. Onbaşlı, M. d’Aquino, G. Prenat, G. Finocchio, L. Lopez-Diaz, R. Chantrell, O. Chubykalo-Fesenko, and P. Bortolotti, “Opportunities and challenges for spintronics in the microelectronics industry,” *Nat. Electron.*, vol. 3, pp. 446–459, Aug 2020.
- [15] R. Gupta, C. Bouard, F. Kammerbauer, J. O. Ledesma-Martin, I. Kononenko, S. Martin, G. Jakob, M. Drouard, and M. Kläui, “Harnessing orbital hall effect in spin-orbit torque mram,” *arXiv preprint arXiv:2404.02821*, 2024.
- [16] D. Go, D. Jo, H.-W. Lee, M. Kläui, and Y. Mokrousov, “Orbitronics: Orbital currents in solids,” *Europhys. Lett.*, vol. 135, p. 37001, sep 2021.
- [17] D. Go, D. Jo, C. Kim, and H.-W. Lee, “Intrinsic spin and orbital hall effects from orbital texture,” *Phys. Rev. Lett.*, vol. 121, p. 086602, Aug 2018.
- [18] D. Jo, D. Go, and H.-W. Lee, “Gigantic intrinsic orbital hall effects in weakly spin-orbit coupled metals,” *Phys. Rev. B*, vol. 98, p. 214405, Dec 2018.
- [19] L. Salemi and P. M. Oppeneer, “First-principles theory of intrinsic spin and orbital hall and nernst effects in metallic monoatomic crystals,” *Phys. Rev. Mater.*, vol. 6, p. 095001, Sep 2022.
- [20] S. Ding, A. Ross, D. Go, L. Baldrati, Z. Ren, F. Freimuth, S. Becker, F. Kammerbauer, J. Yang, G. Jakob, Y. Mokrousov, and M. Kläui, “Harnessing orbital-to-spin conversion of interfacial orbital currents for efficient spin-orbit torques,” *Phys. Rev. Lett.*, vol. 125, p. 177201, Oct 2020.
- [21] Y.-G. Choi, D. Jo, K.-H. Ko, D. Go, K.-H. Kim, H. G. Park, C. Kim, B.-C. Min, G.-M. Choi, and H.-W. Lee, “Observation of the orbital hall effect in a light metal ti,” *Nature*, vol. 619, pp. 52–56, Jul 2023.
- [22] D. Lee, D. Go, H.-J. Park, W. Jeong, H.-W. Ko, D. Yun, D. Jo, S. Lee, G. Go, J. H. Oh, K.-J. Kim, B.-G. Park, B.-C. Min, H. C. Koo, H.-W. Lee, O. Lee, and K.-J. Lee, “Orbital torque in magnetic bilayers,” *Nat. Commun.*, vol. 12, p. 6710, Nov 2021.
- [23] I. Lyalin, S. Alikhah, M. Berritta, P. M. Oppeneer, and R. K. Kawakami, “Magneto-optical detection of the orbital hall effect in chromium,” *Phys. Rev. Lett.*, vol. 131, p. 156702, Oct 2023.
- [24] A. Bose, F. Kammerbauer, R. Gupta, D. Go, Y. Mokrousov, G. Jakob, and M. Kläui, “Detection of long-range orbital-hall torques,” *Phys. Rev. B*, vol. 107, p. 134423, Apr 2023.
- [25] J. O. Ledesma-Martin, E. Galindez-Ruales, S. Krishnia, F. Fuhrmann, D. M. Tran, R. Gupta, M. Gasser,

- D. Go, G. Jakob, Y. Mokrousov, *et al.*, “Non-reciprocity in magnon mediated charge-spin-orbital current interconversion,” *arXiv preprint arXiv:2411.07044*, 2024.
- [26] A. Bose, T. G. Saunderson, A. Shahee, L. Zhang, T. Hajiri, A. Rajan, D. Go, H. Asano, U. Schwingenschlögl, A. Manchon, *et al.*, “Fluctuation-mediated spin-orbit torque enhancement in the noncollinear antiferromagnet $\text{mn}_3\text{ni}_0.35\text{cu}_0.65\text{n}$,” *arXiv preprint arXiv:2401.16021*, 2024.
- [27] H. Hayashi, D. Jo, D. Go, T. Gao, S. Haku, Y. Mokrousov, H.-W. Lee, and K. Ando, “Observation of long-range orbital transport and giant orbital torque,” *Commun. Phys.*, vol. 6, no. 1, p. 32, 2023.
- [28] S. Ding, Z. Liang, D. Go, C. Yun, M. Xue, Z. Liu, S. Becker, W. Yang, H. Du, C. Wang, Y. Yang, G. Jakob, M. Kläui, Y. Mokrousov, and J. Yang, “Observation of the orbital rashba-edelstein magnetoresistance,” *Phys. Rev. Lett.*, vol. 128, p. 067201, Feb 2022.
- [29] S. Krishnia, Y. Sassi, F. Ajejas, N. Sebe, N. Reyren, S. Collin, T. Denneulin, A. Kovács, R. E. Dunin-Borkowski, A. Fert, J.-M. George, V. Cros, and H. Jaffrès, “Large interfacial rashba interaction generating strong spin-orbit torques in atomically thin metallic heterostructures,” *Nano Lett.*, vol. 23, pp. 6785–6791, Aug 2023.
- [30] S. A. Nikolaev, M. Chshiev, F. Ibrahim, S. Krishnia, N. Sebe, J.-M. George, V. Cros, H. Jaffrès, and A. Fert, “Large chiral orbital texture and orbital edelstein effect in co/al heterostructure,” *Nano Lett.*, vol. 24, pp. 13465–13472, Oct 2024.
- [31] A. El Hamdi, J.-Y. Chauleau, M. Boselli, C. Thibault, C. Gorini, A. Smogunov, C. Barreateau, S. Gariglio, J.-M. Triscone, and M. Viret, “Observation of the orbital inverse rashba-edelstein effect,” *Nat. Phys.*, vol. 19, pp. 1855–1860, Dec 2023.
- [32] J. Kim, J. Uzuhashi, M. Horio, T. Senoo, D. Go, D. Jo, T. Sumi, T. Wada, I. Matsuda, T. Ohkubo, S. Mitani, H.-W. Lee, and Y. Otani, “Oxide layer dependent orbital torque efficiency in ferromagnet/cu/oxide heterostructures,” *Phys. Rev. Mater.*, vol. 7, p. L111401, Nov 2023.
- [33] S. Han, H.-W. Ko, J. H. Oh, H.-W. Lee, K.-J. Lee, and K.-W. Kim, “Orbital pumping incorporating both orbital angular momentum and position,” *arXiv preprint arXiv:2311.00362*, 2023.
- [34] D. Go, K. Ando, A. Pezo, S. Blügel, A. Manchon, and Y. Mokrousov, “Orbital pumping by magnetization dynamics in ferromagnets,” *arXiv preprint arXiv:2309.14817*, 2023.
- [35] X. Ning, H. Jaffrès, W. Zhao, and A. Manchon, “Phenomenology of orbital torque, pumping and mixing conductance in metallic bilayers,” *arXiv preprint arXiv:2412.08340*, 2024.
- [36] A. Brataas, Y. Tserkovnyak, G. E. Bauer, and B. I. Halperin, “Spin battery operated by ferromagnetic resonance,” *Phys. Rev. B*, vol. 66, no. 6, p. 060404, 2002.
- [37] Y. Tserkovnyak, A. Brataas, and G. E. Bauer, “Enhanced gilbert damping in thin ferromagnetic films,” *Phys. Rev. Lett.*, vol. 88, no. 11, p. 117601, 2002.
- [38] K. Ando, Y. Kajiwara, S. Takahashi, S. Maekawa, K. Takemoto, M. Takatsu, and E. Saitoh, “Angular dependence of inverse spin-hall effect induced by spin pumping investigated in a ni 81 fe 19/pt thin film,” *Phys. Rev. B*, vol. 78, no. 1, p. 014413, 2008.
- [39] O. Mosendz, J. Pearson, F. Fradin, G. Bauer, S. Bader, and A. Hoffmann, “Quantifying spin hall angles from spin pumping: Experiments and theory,” *Phys. Rev. Lett.*, vol. 104, no. 4, p. 046601, 2010.
- [40] A. Azevedo, L. Vilela-Leão, R. Rodríguez-Suárez, A. Lacerda Santos, and S. Rezende, “Spin pumping and anisotropic magnetoresistance voltages in magnetic bilayers: Theory and experiment,” *Phys. Rev. B*, vol. 83, no. 14, p. 144402, 2011.
- [41] L. Bai, P. Hyde, Y. Gui, C.-M. Hu, V. Vlaminck, J. Pearson, S. Bader, and A. Hoffmann, “Universal method for separating spin pumping from spin rectification voltage of ferromagnetic resonance,” *Phys. Rev. Lett.*, vol. 111, no. 21, p. 217602, 2013.
- [42] K. Ando, S. Takahashi, J. Ieda, H. Kurebayashi, T. Trypiniotis, C. Barnes, S. Maekawa, and E. Saitoh, “Electrically tunable spin injector free from the impedance mismatch problem,” *Nat. Mater.*, vol. 10, no. 9, pp. 655–659, 2011.
- [43] T. S. Seifert, D. Go, H. Hayashi, R. Rouzezar, F. Freimuth, K. Ando, Y. Mokrousov, and T. Kampfrath, “Time-domain observation of ballistic orbital-angular-momentum currents with giant relaxation length in tungsten,” *Nat. Nanotechnol.*, vol. 18, no. 10, pp. 1132–1138, 2023.
- [44] S. Kumar and S. Kumar, “Ultrafast thz probing of nonlocal orbital current in transverse multilayer metallic heterostructures,” *Nat. Commun.*, vol. 14, no. 1, p. 8185, 2023.
- [45] H. Hayashi, D. Go, S. Haku, Y. Mokrousov, and K. Ando, “Observation of orbital pumping,” *Nat. Electron.*, vol. 7, no. 8, pp. 646–652, 2024.
- [46] E. Saitoh, M. Ueda, H. Miyajima, and G. Tatara, “Conversion of spin current into charge current at room temperature: Inverse spin-hall effect,” *Appl. Phys. Lett.*, vol. 88, no. 18, 2006.
- [47] J. C. R. Sánchez, L. Vila, G. Desfonds, S. Gambarelli, J. P. Attané, J. M. De Teresa, C. Magén, and A. Fert, “Spin-to-charge conversion using rashba coupling at the interface between non-magnetic materials,” *Nat. Commun.*, vol. 4, p. 2944, Dec 2013.
- [48] L. Liu, T. Moriyama, D. Ralph, and R. Buhrman, “Spin-torque ferromagnetic resonance induced by the spin hall effect,” *Phys. Rev. Lett.*, vol. 106, no. 3, p. 036601, 2011.
- [49] M. Harder, Y. Gui, and C.-M. Hu, “Electrical detection of magnetization dynamics via spin rectification effects,” *Phys. Rep.*, vol. 661, pp. 1–59, 2016.